Principles of Electron Diffraction Imaging of Defects and Dislocations

S. L. Dudarev

EURATOM/UKAEA Fusion Association, Culham Science Centre
Oxfordshire OX14 3DB, UK

Introduction

In the afternoon of the 3rd of May 1956 at Cavendish Laboratory, Cambridge, England, Mike Whelan and Bob Horne were surprised to see "... the astonishing sight of short-line features dashing about..." in the field of view of the electron microscope that they were using. This was the first observation of dislocations in a metal. The technique that they used was what is now known as bright-field electron microscope imaging. This set of notes explains how a diffraction image of a defect (for example a dislocation or a small dislocation loop) is formed, what determines the limit of spatial resolution of a conventional electron microscope image, and why single point defects in metals have not been observed yet, and how to interpret images of small dislocation loops.

Figure 1: Mike Whelan (centre) with Bob Horne (left) and Chris Jackson (right) in the (old) Cavendish Laboratory, Cambridge, in 1955. J. D. Watson and Francis Crick built their double helix model of DNA in an adjacent room shortly before this photograph was taken.

Figure 2: M. J. Whelan (left) with P. B. Hirsch (right) in Caius College, Cambridge, in the spring of 1960.

Figure 3: M.J. Whelan in his room in Caius College, Cambridge, in 1956.

Fig. 1. Back-reflection microbeam X-ray diffraction pattern of deformed Al (after Hirsch and Kellar, 1952); 422 Debye-Scherrer ring.

8. (*right*) An X-ray photograph of crystalline D N A in the A form

9. (*below*) Elizabeth Watson, with Clare Bridge in the background

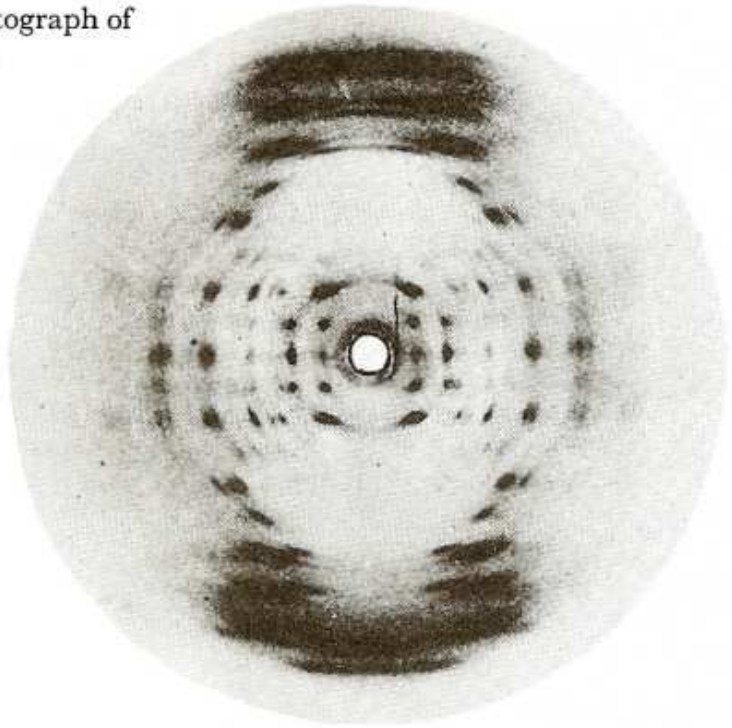

Figure 4: X-ray diffraction patterns used for the identification of dislocation structures (left) and the structure of DNA (right) before the development of electron microscope imaging techniques.

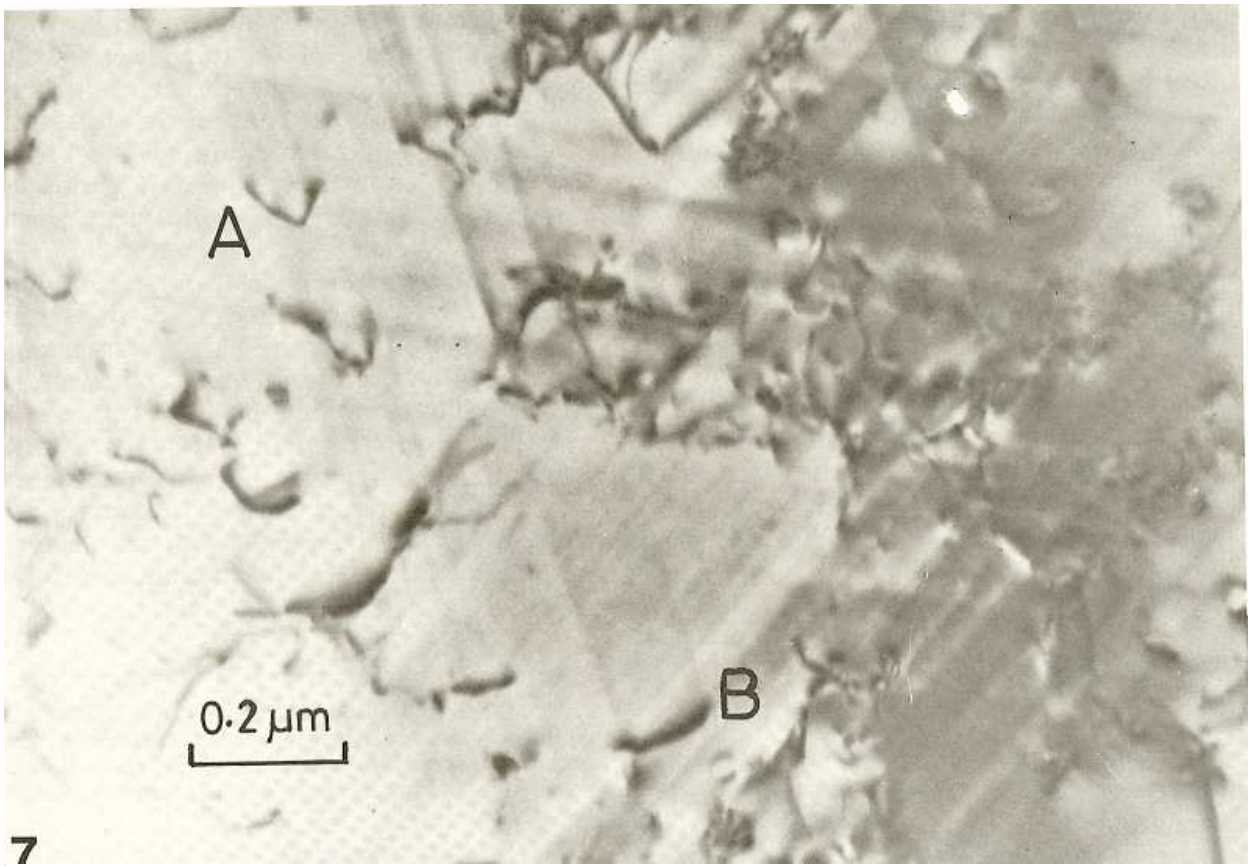

Figure 5: A single crystal aluminium specimen deformed 5% and electropolished, showing bowed dislocations near A and a slip trace behind dislocation B. See P. B. Hirsch, R. W. Horne and M. J. Whelan, *Direct observation of the arrangement and motion of dislocations in aluminium*, Philos. Mag. **1** (1956) 677–684. This photograph was taken in 1956 and published 30 years later in: M.J. Whelan, Journal of Electron Microscopy Technique **3** (1986) 109–129.

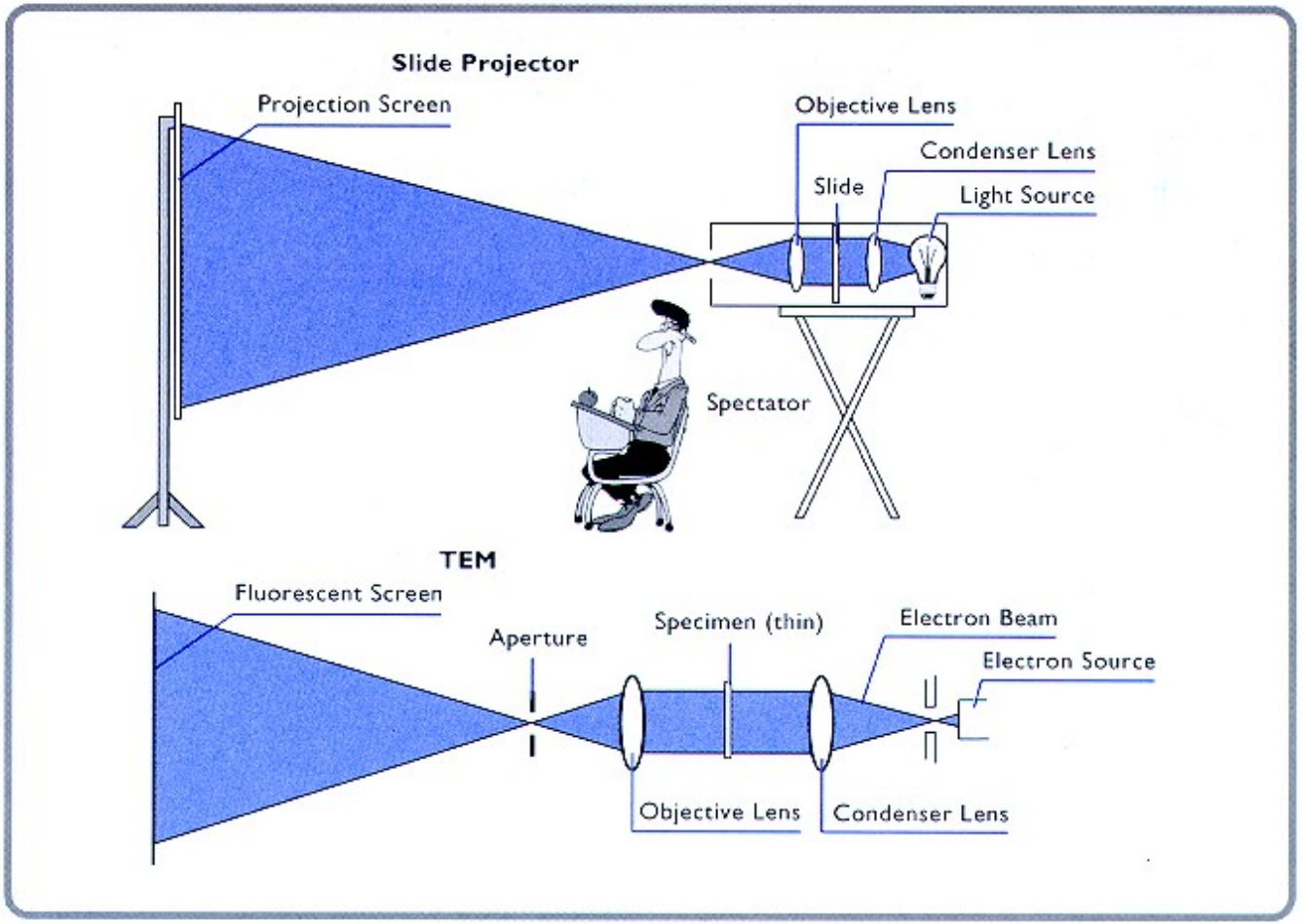

Figure 6: Schematic diagram illustrating the principles of operation of an electron microscope. From http://www.mete.metu.edu.tr/Facilities/Service/TEM/TEMtext/TEMtext.html

Scattering by a Periodic Potential

Electron diffraction imaging, and the interpretation of electron microscope images, relies on the fact that it is possible to find an accurate solution for the Schrödinder equation with a periodic potential describing the interaction of electrons with atoms in a crystal

$$-\frac{\hbar^2}{2m}\nabla\Psi(\mathbf{r})+V(\mathbf{r})\Psi(\mathbf{r})=\frac{\hbar^2\mathbf{k}^2}{2m}\Psi(\mathbf{r})$$

Here $\mathbf{k}$ is the wave vector of a high-energy (~ 100 keV) electron incident on the crystal and m is the mass of the electron. Interaction between the electron and the crystal is described by potential $V(\mathbf{r})$. The potential is a sum of electrostatic fields of electrons and atomic nuclei

$$V(\mathbf{r})=\int\frac{e^2\rho(\mathbf{r})}{|\mathbf{r}-\mathbf{r}'|}-\sum_n\frac{Z_ne^2}{|\mathbf{r}-\mathbf{R}_n|}$$

and is often written as a sum of potentials of individual atoms $V(\mathbf{r})=\sum_n V(\mathbf{r}-\mathbf{R}_n)$.

Scattering by a Periodic Potential

In a perfect crystal the potential $V(\mathbf{r})$ felt by the incident high-energy electrons is a periodic function of $\mathbf{r}$ and hence it can be written as a Fourier series (see for example Marshall and Lovesey (1971))

$$V(\mathbf{r}) = \sum_n V(\mathbf{r} - \mathbf{R}_n) = \sum_{\mathbf{G}} V_{\mathbf{G}} \exp(i\mathbf{G}\cdot\mathbf{r}).$$

Here $\mathbf{G}$'s are the reciprocal lattice vectors. The Schrödinger equation now acquires the form

$$-\frac{\hbar^2}{2m}\nabla\Psi(\mathbf{r}) + \left[\sum_{\mathbf{G}} V_{\mathbf{G}} \exp(i\mathbf{G}\cdot\mathbf{r})\right]\Psi(\mathbf{r}) = \frac{\hbar^2\mathbf{k}^2}{2m}\Psi(\mathbf{r}),$$

where in the vacuum the wave function describing the incident high-energy electrons is $\Psi(\mathbf{r}) = \exp(i\mathbf{k}\cdot\mathbf{r})$. The current density associated with the incident electrons is

$$\mathbf{j}(\mathbf{r}) = \frac{i\hbar}{2m}\left[\Psi(\mathbf{r})\nabla\Psi^*(\mathbf{r}) - \Psi^*(\mathbf{r})\nabla\Psi(\mathbf{r})\right] = \frac{\hbar\mathbf{k}}{m} = \mathbf{v}.$$

This equation shows that wave function $\exp(i\mathbf{k}\cdot\mathbf{r})$ describes a beam of electrons containing one particle per unit volume, all moving with the same velocity $\mathbf{v} = \hbar\mathbf{k}/m$. Obviously $\exp(i\mathbf{k}\cdot\mathbf{r})$ does not satisfy the above Schrödinger equation.

Scattering by a Periodic Potential

The Schrödinger equation is solved by asserting that inside the crystal the wave function is a superposition of Bloch waves

$$\Psi(\mathbf{r}) = \sum_j \alpha_j \sum_{\mathbf{G}} C_{\mathbf{G}j} \exp(i[\mathbf{k}^{(j)} + \mathbf{G}] \cdot \mathbf{r}).$$

The unitary matrix $C_{\mathbf{G}j}$ is found by substituting this form of the solution into the original Schrödinger equation and solving the resulting system of equations for eigenvalues and eigenstates numerically. Coefficients α_j are chosen to satisfy the boundary conditions at the surface where electrons first enter the crystal foil.

A. Howie and M. J. Whelan in 1961 approached the problem from a more practical, and useful, point of view [see Proc. Roy. Soc. (London) **A267** (1961) 217-237]. They thought that the presence of the Fourier components of the potential would result in a *gradual* transformation of the incident plane wave $\exp(i\mathbf{k} \cdot \mathbf{r})$ into a superposition of plane waves of the form

$$\Psi(\mathbf{r}) = \sum_{\mathbf{G}} \phi_{\mathbf{G}}(\mathbf{r}) \exp(i[\mathbf{k} + \mathbf{G}] \cdot \mathbf{r})$$

where the *slowly varying* functions $\phi_{\mathbf{G}}(\mathbf{r})$ would take care of both the effect of periodicity of the crystal and of the boundary conditions.

Scattering by a Periodic Potential

They substituted $\sum_{\mathbf{G}} \phi_{\mathbf{G}}(\mathbf{r}) \exp(i[\mathbf{k}+\mathbf{G}]\cdot\mathbf{r})$ into the Schrödinger equation and found that the set of functions $\{\phi_{\mathbf{G}}(\mathbf{r})\}$ satisfies a closed system of coupled equations

$$i\frac{\hbar^2}{m}[\mathbf{k}+\mathbf{G}]\cdot\nabla\phi_{\mathbf{G}}(\mathbf{r}) = \frac{\hbar^2}{2m}[(\mathbf{k}+\mathbf{G})^2-\mathbf{k}^2]\phi_{\mathbf{G}}(\mathbf{r}) + \sum_{\mathbf{G}'} V_{\mathbf{G}-\mathbf{G}'}\phi_{\mathbf{G}'}(\mathbf{r}).$$

Note that in these equations we neglected the second-order derivatives. This is equivalent to neglecting the effect of *coherent back-scattering* of high-energy electrons from the foil. In the simplest case where we retain only two coupled equations in the above system of equations, we arrive at the famous two-beam Howie-Whelan equations of dynamical electron diffraction.

$$\begin{aligned} i\hbar v\frac{d}{dz}\phi_{\mathbf{0}}(z) &= V_0\phi_{\mathbf{0}}(z) + V_{-\mathbf{G}}\phi_{\mathbf{G}}(z), \\ i\hbar v\frac{d}{dz}\phi_{\mathbf{G}}(z) &= V_0\phi_{\mathbf{G}}(z) + \epsilon_{\mathbf{G}}\phi_{\mathbf{G}}(z) + V_{\mathbf{G}}\phi_0(z). \end{aligned}$$

where

$$\epsilon_{\mathbf{G}} = \frac{\hbar^2}{2m}[(\mathbf{k}+\mathbf{G})^2-\mathbf{k}^2]$$

is a parameter representing the measure of deviation of the wave vector of the diffracted beam $\exp(i[\mathbf{k}+\mathbf{G}]\cdot\mathbf{r})$ from the constant energy surface (the so-called Ewald sphere) $\mathbf{k}^2 = const$.

Dynamical Diffraction of High-Energy Electrons

The boundary conditions for the Howie-Whelan equations are very simple: there is an incident wave and the amplitude of the diffracted wave is zero

$$\begin{aligned} \phi_0(0) &= 1 \\ \phi_{\mathbf{G}}(0) &= 0. \end{aligned}$$

Looking for a solution of the Howie-Whelan equations in the form $\phi_0(z), \phi_{\mathbf{G}}(z) \sim \exp(\lambda z)$ we find a system of two equations determining the values of parameter λ. The *characteristic equation* $\chi(\lambda)$ is given by the formula

$$\chi(\lambda) = \begin{vmatrix} i\hbar\lambda - V_0 & -V_{-\mathbf{G}} \\ -V_{\mathbf{G}} & i\hbar v\lambda - V_0 - \epsilon_{\mathbf{G}} \end{vmatrix} = 0.$$

The roots of this equation are

$$\lambda_{1,2} = -i\frac{V_0}{\hbar v} - \frac{i}{2\hbar v}\left(\epsilon_{\mathbf{G}} \pm \sqrt{\epsilon_{\mathbf{G}}^2 + 4|V_{\mathbf{G}}|^2}\right),$$

and the solutions of the Howie-Whelan equations have the general form

$$\phi_0(z), \phi_{\mathbf{G}}(z) \sim A\exp(\lambda_1 z) + B\exp(\lambda_2 z).$$

Dynamical Diffraction of High-Energy Electrons

Using the boundary conditions we find

$$
\begin{aligned}
\phi_0(z) &= \frac{1}{2}\left(1+\frac{\epsilon}{\sqrt{\epsilon^2+4|V_{\mathbf{G}}|^2}}\right)\exp\left(-i\frac{V_0}{\hbar v}z - i\frac{\epsilon}{\hbar v}z - \frac{iz}{2\hbar v}\sqrt{\epsilon^2+4|V_{\mathbf{G}}|^2}\right)\\
&+ \frac{1}{2}\left(1-\frac{\epsilon}{\sqrt{\epsilon^2+4|V_{\mathbf{G}}|^2}}\right)\exp\left(-i\frac{V_0}{\hbar v}z - i\frac{\epsilon}{\hbar v}z + \frac{iz}{2\hbar v}\sqrt{\epsilon^2+4|V_{\mathbf{G}}|^2}\right)\\
\phi_{\mathbf{G}}(0) &= \frac{V_{-\mathbf{G}}}{\sqrt{\epsilon^2+4|V_{\mathbf{G}}|^2}}\exp\left(-i\frac{V_0}{\hbar v}z - i\frac{\epsilon}{\hbar v}z - \frac{iz}{2\hbar v}\sqrt{\epsilon^2+4|V_{\mathbf{G}}|^2}\right)\\
&- \frac{V_{-\mathbf{G}}}{\sqrt{\epsilon^2+4|V_{\mathbf{G}}|^2}}\exp\left(-i\frac{V_0}{\hbar v}z - i\frac{\epsilon}{\hbar v}z + \frac{iz}{2\hbar v}\sqrt{\epsilon^2+4|V_{\mathbf{G}}|^2}\right).
\end{aligned}
$$

Dynamical Diffraction of High-Energy Electrons

This can be written in a more comprehensible form by using the trigonometric functions $\cos(x) = [\exp(ix) + \exp(-ix)]/2$ and $\sin(x) = [\exp(ix) - \exp(-ix)]/2i$, namely

$$\begin{aligned}
\phi_0(z) &= \exp\left(-i\frac{V_0}{\hbar v}z - i\frac{\epsilon}{\hbar v}z\right)\cos\left(\frac{z}{2\hbar v}\sqrt{\epsilon^2+4|V_{\mathbf{G}}|^2}\right) \\
&+ \frac{i\epsilon}{\sqrt{\epsilon^2+4|V_{\mathbf{G}}|^2}}\exp\left(-i\frac{V_0}{\hbar v}z - i\frac{\epsilon}{\hbar v}z\right)\sin\left(\frac{z}{2\hbar v}\sqrt{\epsilon^2+4|V_{\mathbf{G}}|^2}\right) \\
\phi_{\mathbf{G}}(0) &= -\frac{2iV_{-\mathbf{G}}}{\sqrt{\epsilon^2+4|V_{\mathbf{G}}|^2}}\exp\left(-i\frac{V_0}{\hbar v}z - i\frac{\epsilon}{\hbar v}z\right)\sin\left(\frac{z}{2\hbar v}\sqrt{\epsilon^2+4|V_{\mathbf{G}}|^2}\right).
\end{aligned}$$

This is a important result showing that the amplitude and the intensity of the transmitted and diffracted beams *oscillate* as a function of the thickness of the crystal. This should give rise to thickness fringes seen in electron microscope images of thin crystalline foils, where the thickness of the foil varies across the field of view. Note that the smaller the value of parameter ϵ the higher is the intensity of the diffracted beam.

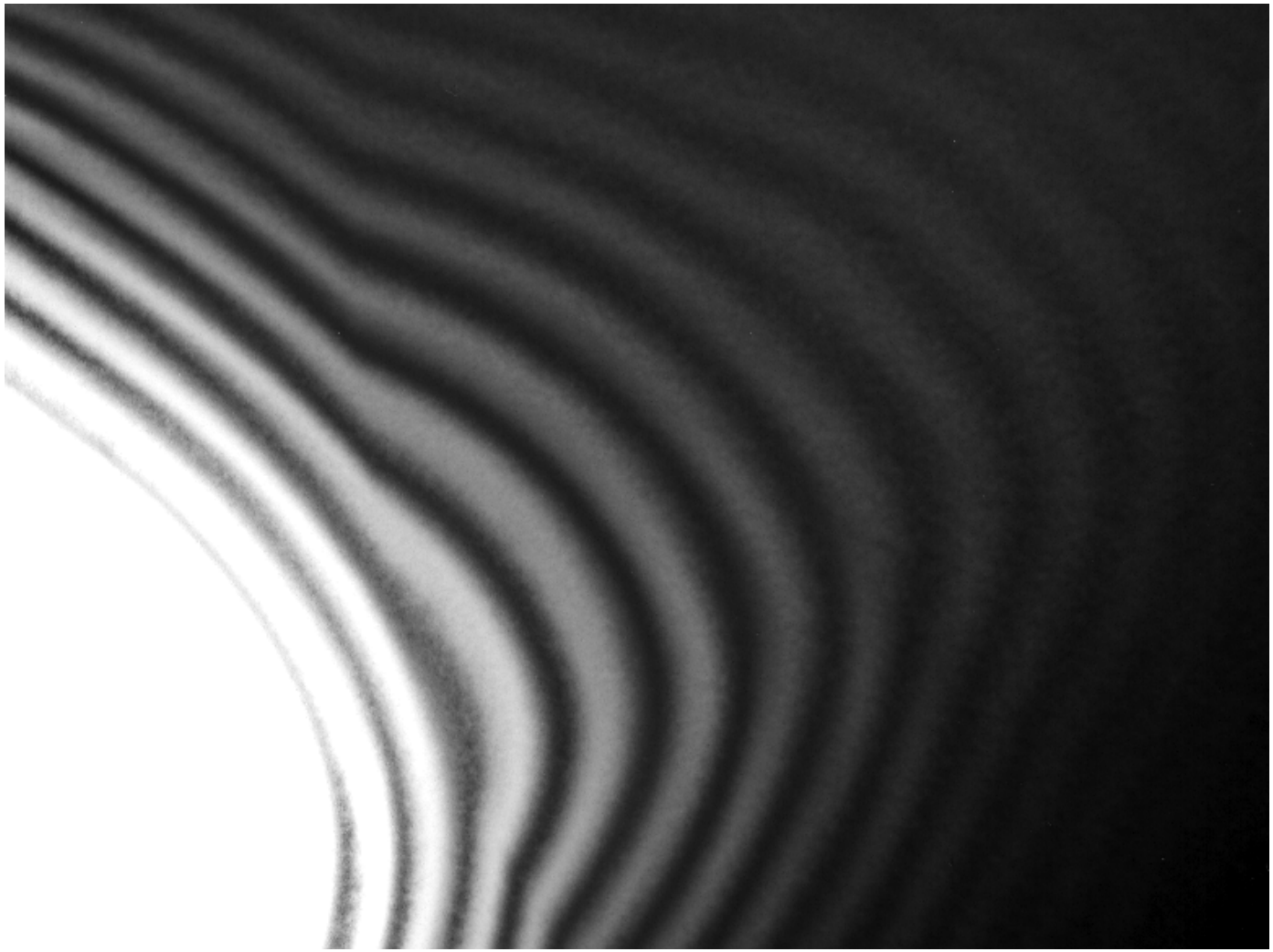

Figure 7: An electron microscope image of the edge of a thin crystal showing thickness fringes resulting from dynamical diffraction of electrons, as described by the Howie-Whelan equations. From http://eml.masc.udel.edu/ gallery.htm

Scattering by a Distorted Crystal

In a distorted crystal (i.e. in a crystal containing a defect, for example a dislocation) the potential $V(\mathbf{r})$ can no longer be treated as a periodic function of coordinate $\mathbf{r}$. In other words, coordinates $\mathbf{R}_n$ no longer form a periodic lattice. If we now evaluate the Fourier component of the potential *using the "old" set of reciprocal lattice vectors* $\mathbf{G}$ we find

$$V_{\mathbf{G}} = \frac{1}{\Omega}\int d\mathbf{r} V(\mathbf{r}-\mathbf{R}_n)\exp(-i\mathbf{G}\cdot\mathbf{r}) = V_{\mathbf{G}}\exp(-i\mathbf{G}\cdot\mathbf{R}_n),$$

where Ω is the volume of a unit cell. In a perfect crystal $\mathbf{G}\cdot\mathbf{R}_n = 2\pi\times(integer)$ and $\exp(-i\mathbf{G}\cdot\mathbf{R}_n) = 1$. In a distorted crystal this is no longer the case, and an approximation often used when describing a distorted crystal, states that the Fourier components of the potential $V_{\mathbf{G}}$ are functions of the *slowly varying* field of atomic displacements

$$V_{\mathbf{G}}(\mathbf{r}) = V_{\mathbf{G}}\exp[-i\mathbf{G}\cdot\mathbf{R}(\mathbf{r})].$$

But is it appropriate to use the field of displacements itself as a physically relevant representation of the defect? The starting point of the theory of elasticity is a statement that the field of displacements is irrelevant, and that it is only the field of the derivatives of displacements $\partial R_i/\partial x_j$ that has any physical significance.

Scattering by a Distorted Crystal

Let's take a look again at the equations for the slowly varying amplitudes of the transmitted and diffracted beams

$$i\frac{\hbar^2}{m}[\mathbf{k}+\mathbf{G}]\cdot\nabla\phi_{\mathbf{G}}(\mathbf{r}) = \frac{\hbar^2}{2m}[(\mathbf{k}+\mathbf{G})^2-\mathbf{k}^2]\phi_{\mathbf{G}}(\mathbf{r})+\sum_{\mathbf{G}'}V_{\mathbf{G}-\mathbf{G}'}\exp\{-i[\mathbf{G}-\mathbf{G}']\cdot\mathbf{R}(\mathbf{r})\}\phi_{\mathbf{G}'}(\mathbf{r}).$$

Since the *phase* of amplitudes $\phi_{\mathbf{G}}(\mathbf{r})$ does not influence the observed intensities of the beams, we can change the definition of these functions by including the phase factor $\exp[-i\mathbf{G}\cdot\mathbf{R}(\mathbf{r})]$, namely

$$\Phi_{\mathbf{G}}(\mathbf{r}) = \phi_{\mathbf{G}}(\mathbf{r})\exp[i\mathbf{G}\cdot\mathbf{R}(\mathbf{r})].$$

The meaning of this gauge transformation is simple. In the original formulation of the problem the direction of propagation of beams was fixed, while the orientation of the crystal varied locally from one point to another. In the new representation the crystal remains "stationary" while the local orientation of the diffracted beams varies. The gauge-transformed equations for the amplitudes have the form

$$i\frac{\hbar^2}{m}[\mathbf{k}+\mathbf{G}]\cdot\nabla\Phi_{\mathbf{G}}(\mathbf{r}) = \frac{\hbar^2}{2m}[(\mathbf{k}+\mathbf{G})^2-\mathbf{k}^2]\Phi_{\mathbf{G}}(\mathbf{r})-\frac{\hbar^2}{m}[\mathbf{k}+\mathbf{G}]\cdot\nabla[\mathbf{G}\cdot\mathbf{R}(\mathbf{r})]\Phi_{\mathbf{G}}(\mathbf{r})+\sum_{\mathbf{G}'}V_{\mathbf{G}-\mathbf{G}'}\Phi_{\mathbf{G}'}(\mathbf{r}).$$

Scattering by a Distorted Crystal

The two-beam Howie-Whelan equations describing scattering by a distorted crystal have the form

$$\begin{aligned} i\hbar v\frac{d}{dz}\Phi_{\mathbf{0}}(z) &= V_0\Phi_{\mathbf{0}}(z) + V_{-\mathbf{G}}\Phi_{\mathbf{G}}(z), \\ i\hbar v\frac{d}{dz}\Phi_{\mathbf{G}}(z) &= V_0\Phi_{\mathbf{G}}(z) + \left(\epsilon_{\mathbf{G}} - \frac{\hbar^2 k}{m}\mathbf{G}\cdot\frac{d}{dz}\mathbf{R}(\mathbf{r})\right)\Phi_{\mathbf{G}}(z) + V_{\mathbf{G}}\Phi_0(z). \end{aligned}$$

where in comparison with the case of diffraction by a perfect crystal the parameter $\epsilon_{\mathbf{G}}$ characterising the deviation of the wave vector of the diffracted beam from the constant energy surface is now a local quantity

$$\epsilon_{\mathbf{G}}(\mathbf{r}) = \frac{\hbar^2}{2m}[(\mathbf{k}+\mathbf{G})^2 - \mathbf{k}^2] - \frac{\hbar^2 k}{m}\mathbf{G}\cdot\frac{d}{dz}\mathbf{R}(\mathbf{r}).$$

From analytical solutions available in the case of a perfect crystal we know that the intensity of the diffracted beam is maximum in the case where $\epsilon = 0$. This fact provides a vital clue for understanding how a diffraction contrast image is formed.

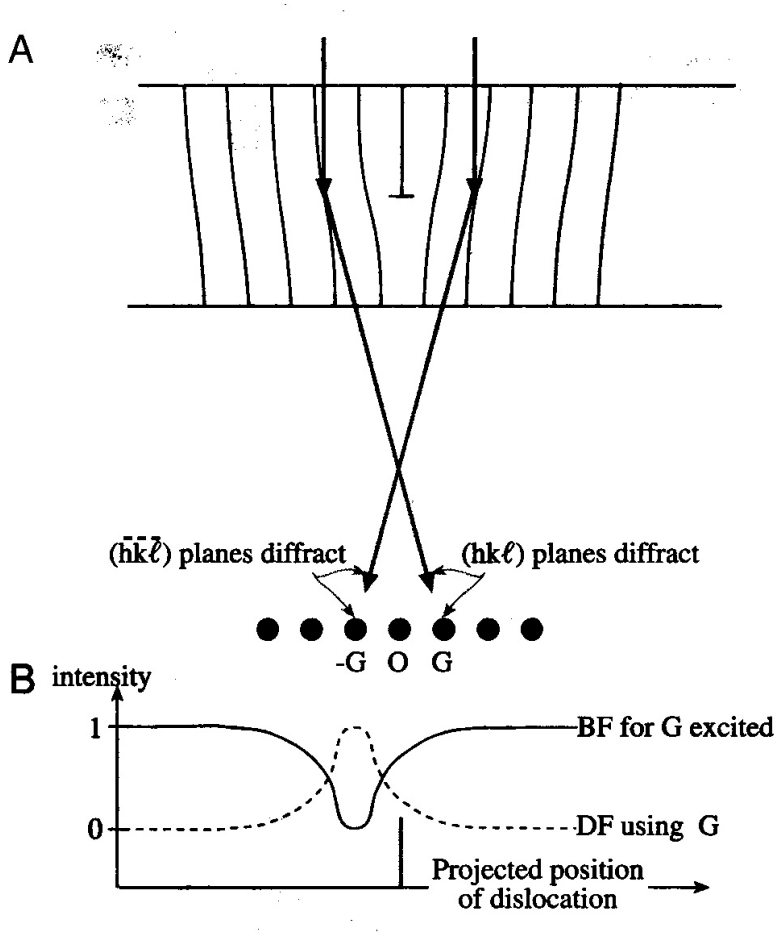

Figure 8: Schematic diagram illustrating the process of formation of a diffraction image. Electrons passing through the centre of a dislocation do not form a strong diffracted beam $\Phi_{\mathbf{G}}$ since all the crystallographic planes have ”wrong” orientation. However electrons incident on atomic planes at the right angle undergo dynamical diffraction and form an intense image.

Weak-Beam Imaging

David Cockayne [D. J. H. Cockayne, I. L. F. Ray and M. J. Whelan, Philos. Mag. **20** (1969) 1265] first noted that the condition

$$\epsilon_{\mathbf{G}}(\mathbf{r}) = \frac{\hbar^2}{2m}[(\mathbf{k}+\mathbf{G})^2 - \mathbf{k}^2] - \frac{\hbar^2 k}{m}\mathbf{G}\cdot\frac{d}{dz}\mathbf{R}(\mathbf{r}) \approx 0$$

should result in an intense dark-field (i.e. obtained using the diffracted rather than transmitted beam) image. If the reciprocal lattice vector $\mathbf{G}$ used for imaging is large, then the width of the region where the above condition is valid is very small, resulting in an image characterized by high spatial resolution. This has led to the development of a new, the so-called weak-beam, method of imaging dislocations and small dislocation loops.

Figure 9: Prof. Lianmao Peng (left) and Prof. David Cockayne (right) at a dinner in Linacre College, Oxford, in November 1996.

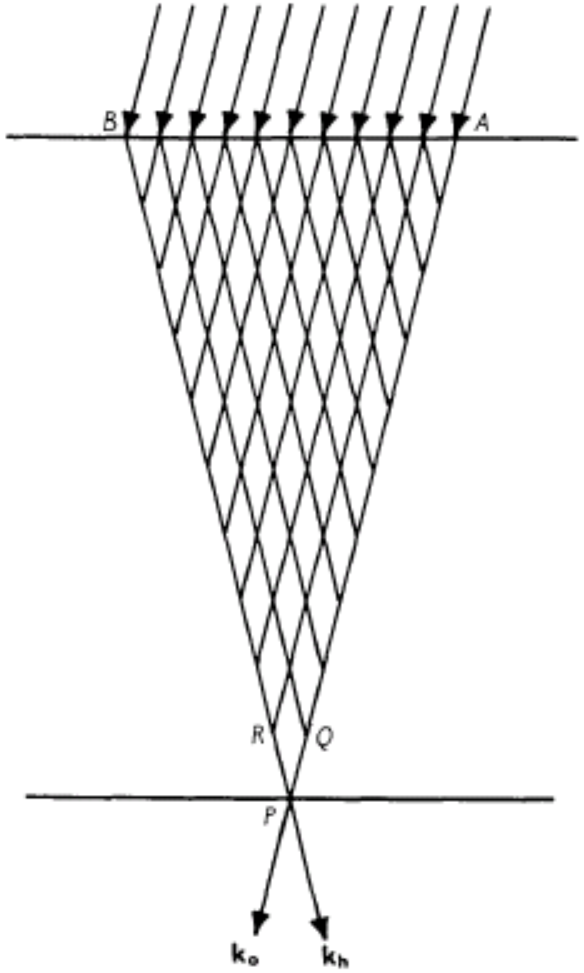

Figure 10: The Takagi triangle (S. Takagi, Acta Crystallographica **15** (1962) 1311) illustrating the limits of validity of the column approximation adopted in the Howie-Whelan equations where the transmitted and the diffracted beams are assumed to propagate in *exactly* the same direction.

The Howie-Basinski Equations

The Takagi triangle sets a limit (or better say an important restrictions) on what can be achieved with conventional diffraction imaging. For example, interpreting images of objects that have the size smaller than

$$D < L\frac{G}{k} = L\frac{\lambda}{a}$$

requires taking into account the fact that the direction of propagation of diffracted beams depends on the reciprocal lattice vector associated with the beam. Here D is the size of the object, L is the thickness of the crystal, λ is the wavelength of electrons ($\lambda = 0.037$Å for 100 keV electrons) and a is the distance between atomic planes. For $L = 500$ Å; and $a = 2.5$ Å we find that $D < 7.5$ Å. The effect of non-parallel propagation of diffracted beams is taken into account by using the many-beam Howie-Basinski equations

$$i\frac{\hbar^2}{m}[\mathbf{k}+\mathbf{G}]\cdot\nabla\Phi_{\mathbf{G}}(\mathbf{r}) = \frac{\hbar^2}{2m}[(\mathbf{k}+\mathbf{G})^2-\mathbf{k}^2]\Phi_{\mathbf{G}}(\mathbf{r})-\frac{\hbar^2}{m}[\mathbf{k}+\mathbf{G}]\cdot\nabla[\mathbf{G}\cdot\mathbf{R}(\mathbf{r})]\Phi_{\mathbf{G}}(\mathbf{r})+\sum_{\mathbf{G}'}V_{\mathbf{G}-\mathbf{G}'}\Phi_{\mathbf{G}'}(\mathbf{r}).$$

These equations were derived by A. Howie and Z. S. Basinski in Philosophical Magazine **17** (1968) 1039.

Numerical Implementation

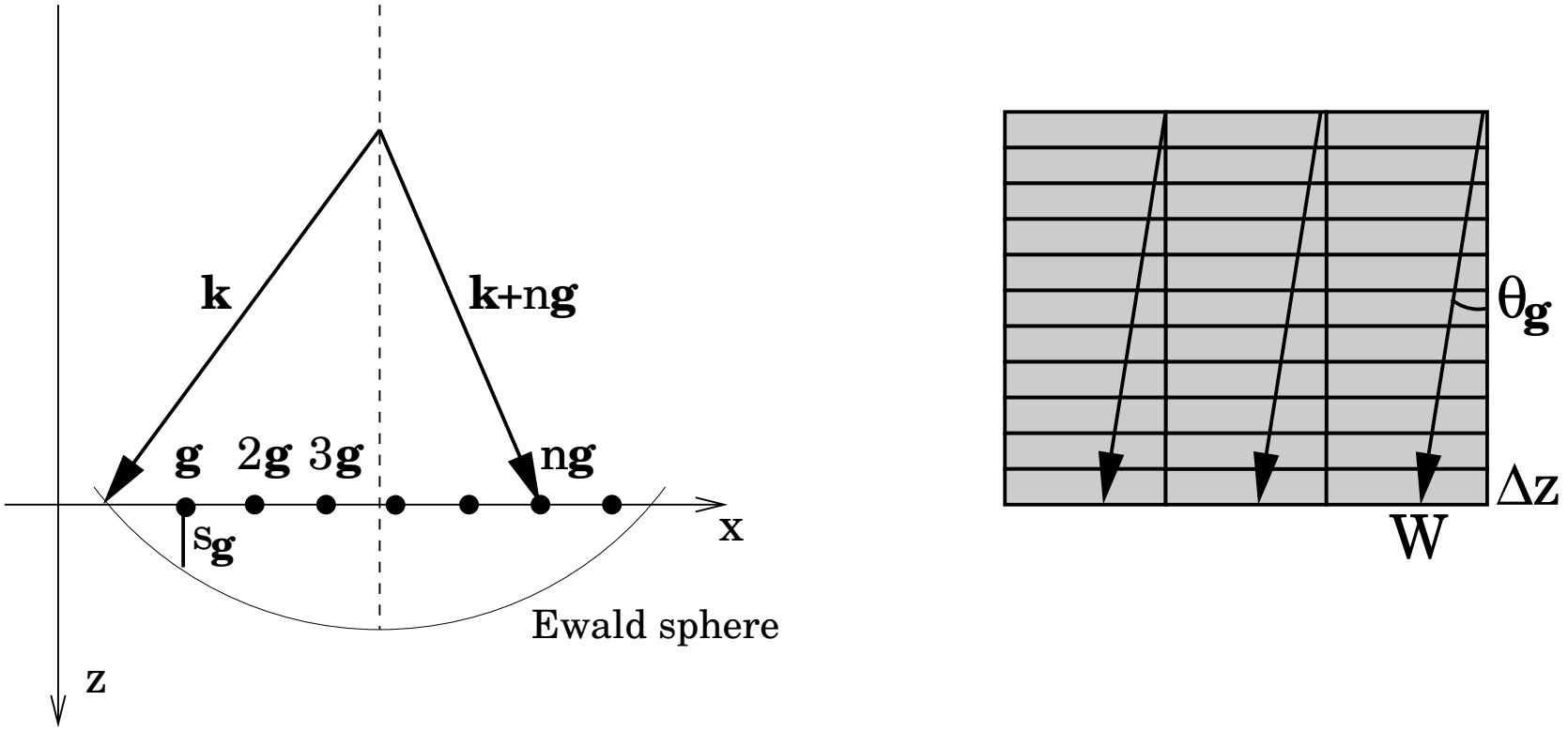

Figure 11: Schematic diagram illustrating the geometry of diffraction conditions. The vertical broken line represents the zone axis, $\mathbf{g}$ is a reciprocal lattice vector and $\mathbf{k}$ is the wave vector of the incident beam of electrons. The geometry of diffraction illustrated in this figure corresponds to a weak-beam condition typically used in electron microscope imaging where the sphere of constant energy *does not* pass through a reciprocal lattice point.

Numerical Implementation

The idea is to use the Howie-Whelan equations to propagate the diffracted beams along the zone axis, and to take account of the *inclined* propagation by equating beam amplitudes entering a slice normal the zone axis to linear combinations of beam amplitudes exiting adjacent cells in the previous slice.

$\Phi_{g'}^{(in)}(\nu, z)$ and $\Phi_{g'}^{(out)}(\nu, z + \Delta z)$ are the amplitudes of the diffracted beam $\mathbf{k} + \mathbf{g}'$ entering and exiting the ν'th cell of the slice at z of thickness Δz.

Within each slice there are rows of cells along the x-axis and ν increases along each row and from one row to the next along the y-axis. θ'_g denote the angle between the diffracted beam $\mathbf{k} + \mathbf{g}'$ and the zone axis. The angle θ'_g is in the (x, z) plane, and

$$\tan\theta_{g'} = \frac{(\mathbf{k}+\mathbf{g}')_x}{(\mathbf{k}+\mathbf{g}')_z} \approx \frac{(\mathbf{k}+\mathbf{g}')_x}{(\mathbf{k}+\mathbf{g}'+\mathbf{s}'_{\mathbf{g}})_z}. \quad (1)$$

Numerical Implementation

In the column approximation the amplitude $\Phi_{g'}^{(out)}(\nu, z+\Delta z)$ exiting the ν'th cell of a given slice equals the amplitude $\Phi_{g'}^{(in)}(\nu, z+\Delta z)$ entering the ν'th cell of the next slice. For the inclined propagation the amplitude entering the ν'th cell of the next slice is set equal to a weighted average of the amplitudes exiting the cell directly above and an adjacent cell:

$$\Phi_{g'}^{(in)}(\nu, z+\Delta z) = \left(1 - \frac{\Delta z}{W}\tan\theta_{g'}\right)\Phi_{g'}^{(out)}(\nu, z+\Delta z) + \left(\frac{\Delta z}{W}\tan\theta_{g'}\right)\Phi_{g'}^{(out)}(\nu-1, z+\Delta z), \tag{2}$$

if $\theta_{g'}$ is positive and

$$\Phi_{g'}^{(in)}(\nu, z+\Delta z) = \left(1 + \frac{\Delta z}{W}\tan\theta_{g'}\right)\Phi_{g'}^{(out)}(\nu, z+\Delta z) - \left(\frac{\Delta z}{W}\tan\theta_{g'}\right)\Phi_{g'}^{(out)}(\nu+1, z+\Delta z), \tag{3}$$

if $\theta_{g'}$ is negative. W is the length of a cell along x.

This finite difference method is fully equivalent to the set of couple differential equations of dynamical diffraction. Hence it provides a way of simulating images of defects for an arbitrary configuration of displacements of atoms.

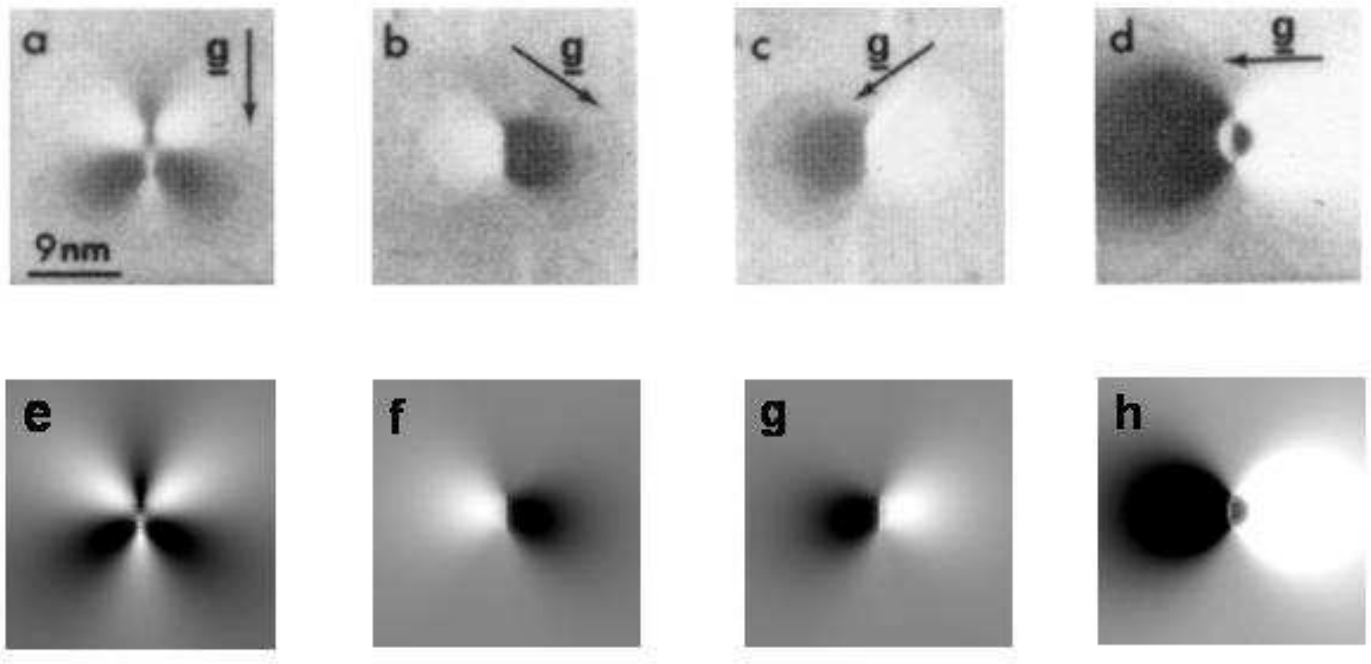

Figure 12: Simulated dark-field images of a perfect dislocation loop with $\mathbf{b} = 1/2[01\bar{1}]$ under two-beam dynamical conditions. The original images of Eyre *et al.* (1977) are shown above ((a) to (d)) and simulated images are shown below ((e)-(h)). (a) and (e) $\mathbf{g} = 200$, $\mathbf{g} \cdot \mathbf{b} = 0$; (b) and (f) $\mathbf{g} = 11\bar{1}$, $\mathbf{g} \cdot \mathbf{b} = 1$; (c) and (g) $\mathbf{g} = 1\bar{1}1$, $\mathbf{g} \cdot \mathbf{b} = 1$; (d) and (h) $\mathbf{g} = 0\bar{2}2$, $\mathbf{g} \cdot \mathbf{b} = 2$. Loop diameter is ~ 5 nm. Foil thickness and loop depth are set according to Eyre *et al.* (1977). From Z. Zhou *et al.* Philos. Mag. (2006) in press

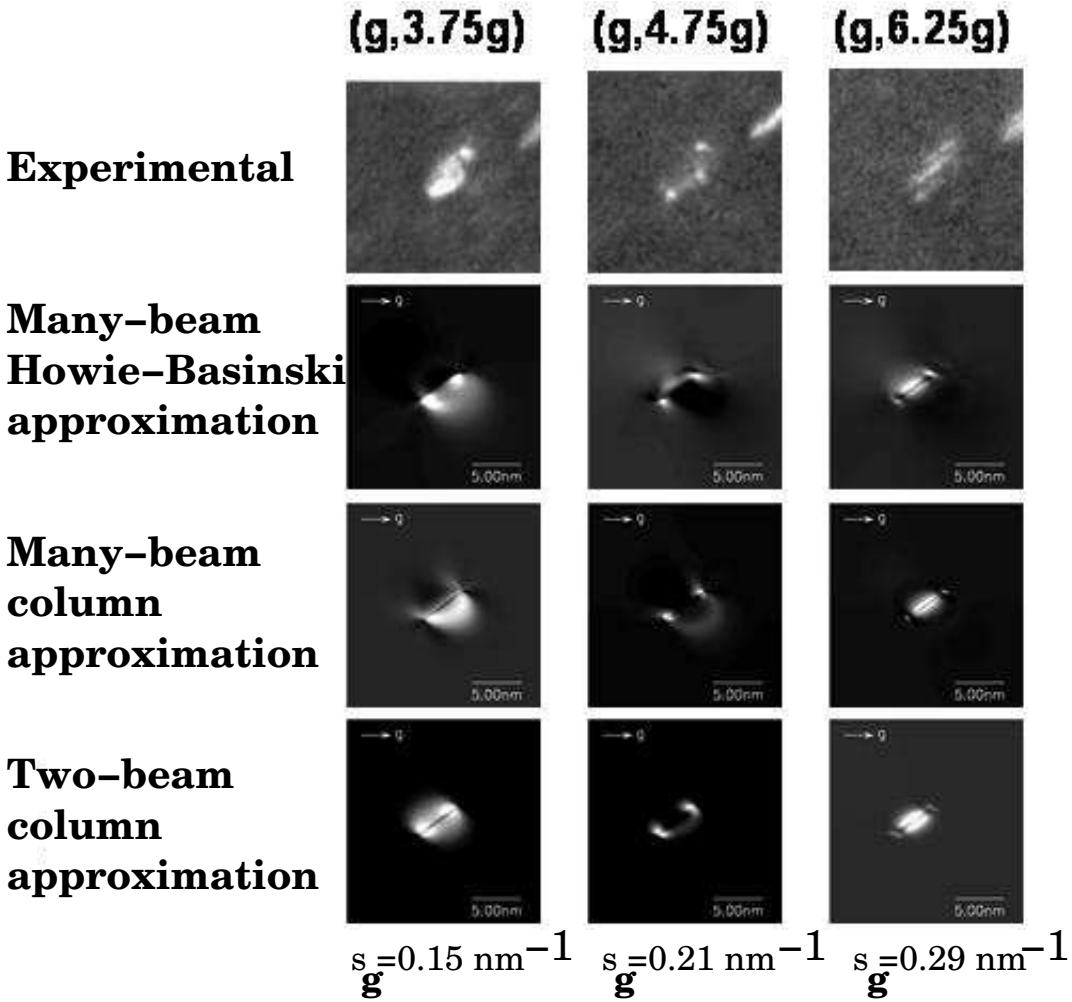

Figure 13: Simulated and experimental weak-beam images of edge-on loops in copper. The electron energy is 100 keV, and the beam direction is close to $[110]$. The loop diameter in the simulated images is 5 nm, foil thickness 60 nm, loop depth 30 nm and $s_{\mathbf{g}}$ is the deviation parameter.

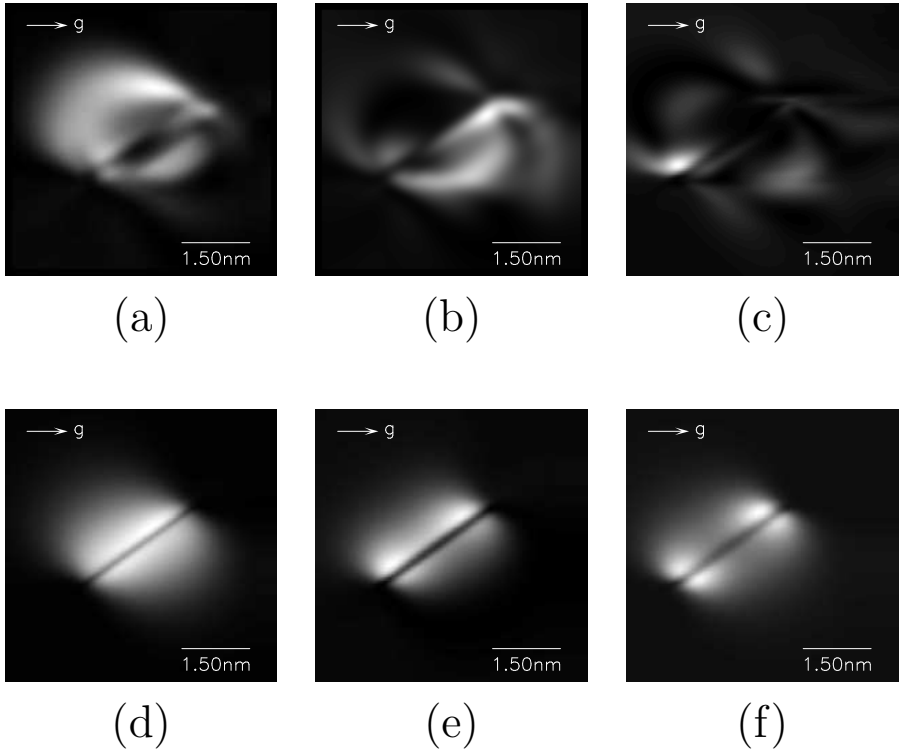

Figure 14: Simulated weak-beam images of an edge-on loop of diameter 3 nm in copper for $\mathbf{g} = 002$ at the $[110]$ pole. Foil thickness $t = 60$ nm. Loops are located around the centre of the foil. Weak-beam condition (a) & (d) $(\mathbf{g}, 4.0\mathbf{g})$, (b) & (e) $(\mathbf{g}, 5.0\mathbf{g})$, (c) & (f) $(\mathbf{g}, 6.0\mathbf{g})$; (a), (b) & (c) eight beams ($0\mathbf{g}$ - $7\mathbf{g}$) approximation; (d), (e) & (f) two-beam approximation for the same deviation parameters $|\mathbf{s}_{\mathbf{g}}|$. The many-beam calculations show that undesirable fine structure can occur if images are formed under dynamical diffraction conditions involving strong interference between several reflections belonging to a systematic row.

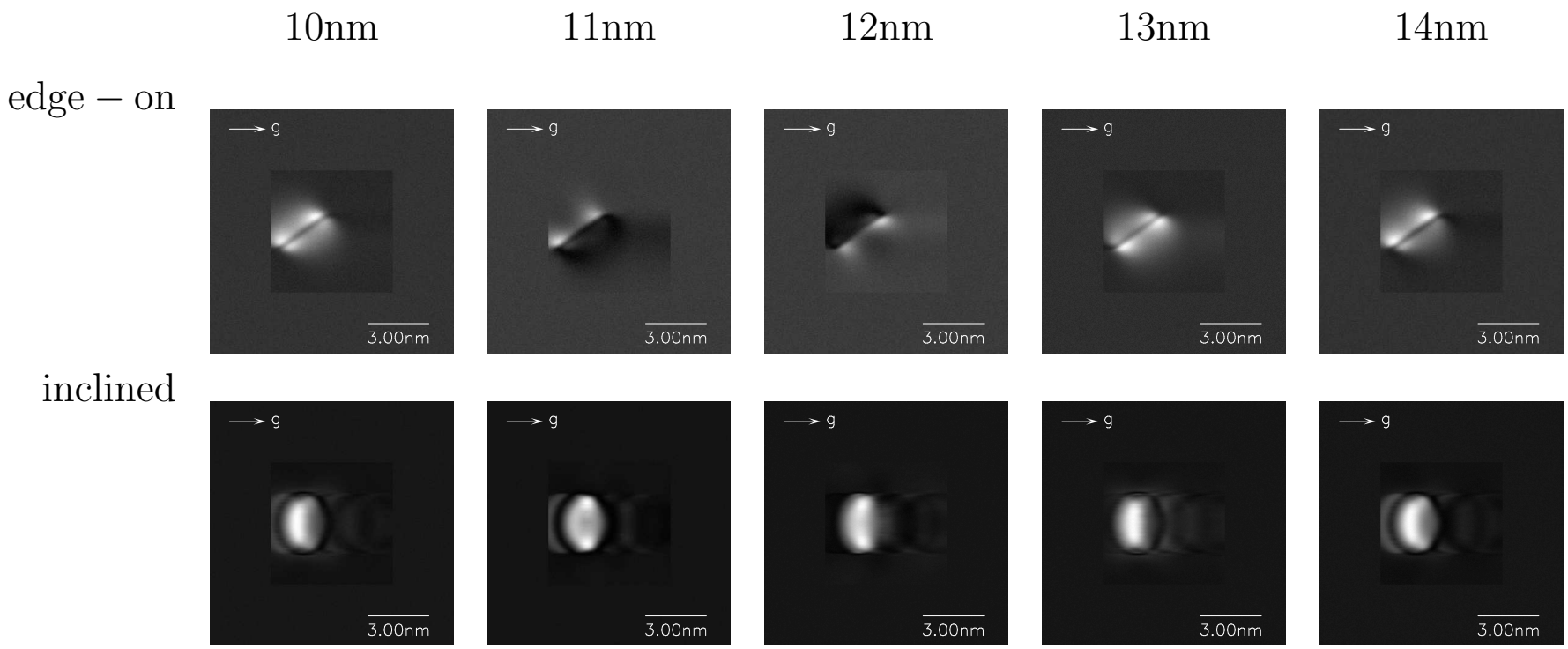

Figure 15: Simulated weak-beam images of edge-on and inclined loops of diameter 3 nm. The images from left to right are according to the depth of loops in the foil. Foil thickness is 60 nm and $\mathbf{g} = 002$.

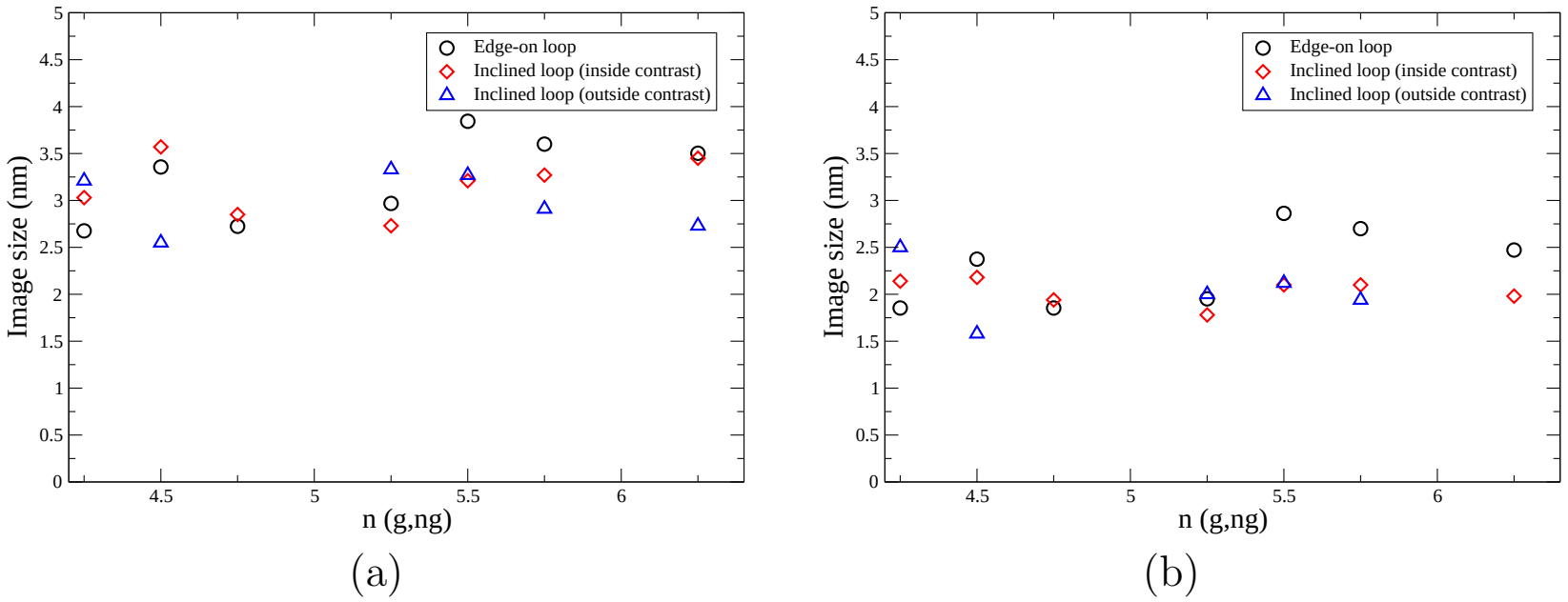

Figure 16: The image size measured from simulated and experimental images of dislocation loops under different weak-beam conditions. (a) and (b) are size measurements from simulated images for loops of diameter 3 nm and 2 nm separately. Note the fluctuations of the apparent image size occurring on the 1nm scale. The effective size of a single interstitial defect is $\sim 0.3nm$.

Bibliography

W. Marshall and S. W. Lovesey, *Theory of Thermal Neutron Scattering*, Clarendon Press, Oxford (1971).

P. B. Hirsch, A. Howie, R. B. Nicholson, D. W. Pashley and M. J. Whelan, *Electron Microscopy of Thin Crystals*, London: Butterworth (1965), there is a new edition by Krieger, Malabar, Florida.

C. J. Humphreys, editor, *Understanding Materials*, A Festschrift for Sir Peter Hirsch, Maney Publishing (2002), ISBN 1-902253-58-0

L.-M. Peng, S. L. Dudarev and M. J. Whelan, *High-Energy Electron Diffraction and Microscopy*, Oxford University Press (2004)

Z.Zhou, M. L. Jenkins, S. L. Dudarev, A. P. Sutton and M. A. Kirk, *Simulations of weak-beam diffraction contrast images of dislocation loops by the many-beam HowieBasinski equations*, Philosophical Magazine **86** (2006) pp. 4851-4881

Z. Zhou, S.L. Dudarev, M.L. Jenkins, A.P. Sutton, M.A. Kirk, *Diffraction imaging and diffuse scattering by small dislocation loops*, Journal of Nuclear Materials **367-370** (2007) pp. 305-310

Acknowledgements

The author is grateful to Professor M. J. Whelan FRS for permission to reproduce photographs illustrating these notes. This work was funded jointly by the United Kingdom Engineering and Physical Sciences Research Council and by the European communities under the Contract of Association between Euratom and UKAEA. The views and opinions expressed herein do not necessarily reflect those of the European Commission.